

Neutron transition strengths of 2_1^+ states in the neutron rich Oxygen isotopes determined from inelastic proton scattering

Nguyen Dang Chien^{1,2} and Dao T. Khoa^{1*}

¹*Institute for Nuclear Science & Technique, VAEK
179 Hoang Quoc Viet Rd., Nghia Do, Hanoi, Vietnam.*

²*Department of Physics, Dalat University
1 Phu Dong Thien Vuong Str., Dalat, Vietnam.*

(Dated: March 13, 2019)

Abstract

A coupled-channel analysis of the $^{18,20,22}\text{O}(p, p')$ data has been performed to determine the neutron transition strengths of 2_1^+ states in Oxygen targets, using the microscopic optical potential and inelastic form factor calculated in the folding model. A complex density- and *isospin* dependent version of the CDM3Y6 interaction was constructed, based on the Brueckner-Hatree-Fock calculation of nuclear matter, for the folding model input. Given an accurate isovector density dependence of the CDM3Y6 interaction, the isoscalar (δ_0) and isovector (δ_1) deformation lengths of 2_1^+ states in $^{18,20,22}\text{O}$ have been extracted from the folding model analysis of the (p, p') data. A specific N -dependence of δ_0 and δ_1 has been established which can be linked to the neutron shell closure occurring at N approaching 16. The strongest isovector deformation was found for 2_1^+ state in ^{20}O , with δ_1 about 2.5 times larger than δ_0 , which indicates a strong core polarization by the valence neutrons in ^{20}O . The ratios of the neutron/proton transition matrix elements (M_n/M_p) determined for 2_1^+ states in $^{18,20}\text{O}$ have been compared to those deduced from the mirror symmetry, using the measured $B(E2)$ values of 2_1^+ states in the proton rich ^{18}Ne and ^{20}Mg nuclei, to discuss the isospin impurity in the 2_1^+ excitation of the $A = 18, T = 1$ and $A = 20, T = 2$ isobars.

PACS numbers: 24.10.Eq, 24.10.Ht, 25.40.Ep, 25.60.-t, 21.10.Re, 21.60.Ev

*Electronic address: khoa@vaec.gov.vn

I. INTRODUCTION

Inelastic proton scattering has been used over decades as a very efficient tool to yield the nuclear structure information. In difference from the electromagnetic probes, protons interact strongly with both protons and neutrons in the target nucleus, and the neutron and proton transition strengths of a nuclear excitation could be reliably deduced from the (p, p') measurement, in terms of the neutron M_n and M_p matrix elements [1]. The knowledge of M_n and M_p can shed light into the relative contributions by the valence nucleons and the core to the nuclear excitation, and hence, provides important information on the core polarization by the valence nucleons which could eventually lead to changes in the shell structure. This topic has recently become of significant interest in the experimental studies with radioactive beams where the inelastic proton scattering can be accurately measured, in the inverse kinematics, for the short-lived unstable nuclei (see, e.g., Refs. [2, 3, 4, 5, 6] for the (p, p') measurements with the unstable Oxygen isotopes). With large neutron (or proton) excess in the unstable nuclei, such proton scattering data provide also a vital information for studying the isospin effects in the proton-nucleus interaction. Although the isospin dependence of the nucleon optical potential (OP), known by now as Lane potential [7], has been studied since a long time, few attempts were made to study the isospin dependence of the transition potential or form factor (FF) for *inelastic* scattering. As neutron and proton contribute differently to the nuclear excitation, the inelastic scattering FF contains also an isospin dependence [8] which determines the degree of the *isovector* mixing in the inelastic scattering channel that induces the excitation [12].

In general, the isospin-dependent part of the nucleon-nucleus OP is proportional to the product of the projectile and target isospins, and the total OP can be written in terms of the *isoscalar* (IS) and *isovector* (IV) components [7] as

$$U(R) = U_0(R) \pm \varepsilon U_1(R), \quad \varepsilon = (N - Z)/A, \quad (1)$$

where the + sign pertains to incident neutron and - sign to incident proton. The strength of the Lane potential U_1 is known from (p, p) and (n, n) elastic scattering and (p, n) reactions studies, to be around 30-40% of the U_0 strength. In the first order of the collective model, inelastic nucleon-nucleus scattering cross section can be reasonably described, in the distorted-wave Born approximation (DWBA) or coupled channel (CC) formalism, with the

inelastic form factor F given by ‘deforming’ the optical potential (1) as

$$F(R) = \delta \frac{dU(R)}{dR} = \delta_0 \frac{dU_0(R)}{dR} \pm \varepsilon \delta_1 \frac{dU_1(R)}{dR}. \quad (2)$$

The explicit knowledge of the deformation lengths δ_0 and δ_1 would give us important structure information about the IS and IV transition strengths of the nuclear excitation under study. There are only two types of experiment that might allow one to determine δ_0 and δ_1 using prescription (2):

i) Charge exchange (p, n) reaction leading to the *excited* isobar analog state. It was shown, however, that the calculated inelastic (p, n) cross sections were insensitive to δ_1 due to the dominance of two-step process [9].

ii) Another way is to extract $\delta_{0(1)}$ from the (p, p') and (n, n') data measured at about the same energy for the same excited state of the target [8, 9]. Since $\varepsilon U_1/U_0$ is only about few percent, the uncertainty of this method can be quite large. Moreover, it remains technically not feasible to perform simultaneously (p, p') and (n, n') measurements in the inverse kinematics for unstable nuclei.

From a theoretical point of view, the form factor (2) has been shown to have inaccurate radial shape which tends to underestimate the transition strength, especially, for high-multipole excitations induced by inelastic heavy-ion scattering [10, 11]. As an alternative, a compact approach based on the folding model has been suggested in Ref. [12] for the determination of the IS and IV transition strengths of the $(\Delta S = \Delta T = 0)$ nuclear excitations induced by inelastic proton scattering. This compact folding approach was used with some success in the DWBA analyses of the $^{30-40}\text{S}(p, p')$ and $^{18-22}\text{O}(p, p')$ data measured in the inverse kinematics, to determine δ_0 and δ_1 for the 2_1^+ states in the Sulfur and Oxygen isotopes under study [12, 13]. We recall that the basic inputs for such a folding + DWBA analysis are the effective NN interaction between the incident proton and those bound in the target, and the transition densities of the nuclear excitation. Consequently, for a carefully chosen model of the nuclear transition densities, the more accurate the choice of the effective NN interaction the more reliable the deduced δ_0 and δ_1 deformation lengths.

Our first folding model analysis of the $^{18,20}\text{O}(p, p')$ data [12] has used a well-tested CDM3Y6 density dependent interaction [14] to construct the proton-nucleus OP and inelastic FF. For simplicity, the density dependence of the isovector part of the CDM3Y6 interaction has been assumed in Ref. [12], following a Hartree-Fock (HF) study of asymmet-

ric nuclear matter [15], to be the same as that of the isoscalar part. As a result, quite a strong IV mixing was found for 2_1^+ states in $^{18,20}\text{O}$, with the ratio of neutron/proton transition matrix elements $M_n/M_p \simeq 4.2$ for ^{20}O . Although that value agrees fairly with previous estimates [2, 3, 4] within the limits of experimental errors, a recent measurement of the Coulomb excitation of ^{20}Mg [6] has revealed that the M_n/M_p is only around 2.5 for 2_1^+ state in ^{20}O , if one assumes the M_p moment of 2_1^+ state in ^{20}Mg equal the M_n moment of 2_1^+ state in ^{20}O based on the isospin symmetry. A question was raised in Ref. [6] whether such a discrepancy is due to the inaccuracy of the (p, p') analysis method of Ref. [12] or the isospin impurity in the 2_1^+ excitation of ^{20}Mg and ^{20}O .

In the mean time, the isovector density dependence of the CDM3Y6 interaction has been carefully probed in the CC analysis of the (p, n) reactions exciting the 0^+ isobaric analog states of ^6He [16] and other medium-mass nuclei including ^{208}Pb [17], where the isovector coupling was used to explicitly link the isovector part of the nucleon OP to the cross section of (p, n) reaction. In particular, a complex isovector density dependence of the CDM3Y6 interaction has been constructed based on the microscopic Brueckner-Hartree-Fock calculation of nuclear matter [18] by Jeukenne, Lejeune and Mahaux (JLM) before being used as folding input. The main conclusion drawn from the results of Refs. [16, 17] is that the strength the isovector density dependence of the CDM3Y6 interaction, even after it was fine tuned against the JLM results, is somewhat weak compared to the empirical isovector strength implied by the (p, n) data. As a result, a renormalization of the (real) isovector density dependence of the CDM3Y6 interaction by a factor of 1.2 - 1.3 was found [17] necessary to account for the measured (p, n) cross sections. Such an enhancement of the isovector density dependence of the CDM3Y6 interaction was also shown [16, 17] necessary for a good HF description of the nuclear matter symmetry energy compared to the empirical estimates.

Since a realistic isospin dependence of the effective NN interaction is vital for the determination of the IS and IV deformation lengths (or M_n and M_p moments), a *revised* folding model analysis of the $^{18,20,22}\text{O}(p, p')$ data is necessary for a more definitive conclusion on the neutron transition strength of 2_1^+ states in $^{18,20,22}\text{O}$ isotopes. After a brief overview of the theoretical formalism in Sec. II, the results of the folding + CC analysis of the $^{18,20,22}\text{O}(p, p')$ data are presented in Sec. III and the main conclusions are given in the Summary.

II. GENERAL FORMALISM

A. Nuclear densities, isoscalar and isovector deformations

We describe here briefly the method suggested first in Ref. [12] to link the deformation of an excited nucleus and the corresponding transition density based on a *collective model* treatment. As the nuclear deformation is associated with the ‘deformed’ shape of excited nucleus, instead of ‘deforming’ the optical potential (2), one can build up the proton and neutron transition densities of a 2^λ -pole excitation ($\lambda \geq 2$) using the so-called Bohr-Mottelson (BM) prescription [19] separately for protons and neutrons

$$\rho_\lambda^\tau(r) = -\delta_\tau \frac{d\rho_{g.s.}^\tau(r)}{dr}, \text{ with } \tau = p, n. \quad (3)$$

Here $\rho_{g.s.}^\tau(r)$ are the proton and neutron ground state (g.s.) densities and δ_τ the corresponding deformation lengths. Given an appropriate choice of the g.s. proton and neutron densities it is natural to represent the IS and IV parts of the total g.s. density as

$$\rho_{g.s.}^{0(1)}(r) = \rho_{g.s.}^n(r) \pm \rho_{g.s.}^p(r). \quad (4)$$

One can then generate, using the same BM prescription, the IS and IV parts of the nuclear transition density by deforming (4) as

$$\rho_\lambda^{0(1)}(r) = -\delta_{0(1)} \frac{d[\rho_{g.s.}^n(r) \pm \rho_{g.s.}^p(r)]}{dr}. \quad (5)$$

The explicit expressions for the IS and IV deformation lengths are then easily obtained, after some integration in parts, as

$$\delta_0 = \frac{N \langle r^{\lambda-1} \rangle_n \delta_n + Z \langle r^{\lambda-1} \rangle_p \delta_p}{A \langle r^{\lambda-1} \rangle_A}, \quad (6)$$

$$\delta_1 = \frac{N \langle r^{\lambda-1} \rangle_n \delta_n - Z \langle r^{\lambda-1} \rangle_p \delta_p}{N \langle r^{\lambda-1} \rangle_n - Z \langle r^{\lambda-1} \rangle_p}. \quad (7)$$

Here the radial momenta $\langle r^{\lambda-1} \rangle_x$ ($x = n, p, A$) are obtained with the neutron, proton and total g.s. densities as

$$\langle r^{\lambda-1} \rangle_x = \int_0^\infty \rho_{g.s.}^x(r) r^{\lambda+1} dr / \int_0^\infty \rho_{g.s.}^x(r) r^2 dr. \quad (8)$$

The transition matrix element associated with a given component of nuclear transition density ($y = n, p, 0, 1$) is

$$M_y = \int_0^\infty \rho_\lambda^y(r) r^{\lambda+2} dr. \quad (9)$$

The ratios of the neutron/proton and IS/IV transition matrix elements are given by

$$\frac{M_n}{M_p} = \frac{N \langle r^{\lambda-1} \rangle_n \delta_n}{Z \langle r^{\lambda-1} \rangle_p \delta_p}, \quad (10)$$

$$\frac{M_1}{M_0} = \frac{(N \langle r^{\lambda-1} \rangle_n - Z \langle r^{\lambda-1} \rangle_p) \delta_1}{(A \langle r^{\lambda-1} \rangle_A) \delta_0}. \quad (11)$$

It is useful to note that there is a one-to-one correspondence between the ratios of transition matrix elements in the two representations, and they are related by

$$M_n/M_p = (1 + M_1/M_0)/(1 - M_1/M_0). \quad (12)$$

If one assumes that the excitation is purely *isoscalar* and the neutron and proton densities have the same radial shape (scaled by the ratio N/Z) then $\delta_n = \delta_p = \delta_0 = \delta_1$,

$$\frac{M_n}{M_p} = \frac{N}{Z} \quad \text{and} \quad \frac{M_1}{M_0} = \frac{N - Z}{A} = \varepsilon. \quad (13)$$

Consequently, any significant deviation of the M_n/M_p ratio from N/Z (or deviation of the M_1/M_0 ratio from ε) would directly indicate an isovector mixing in the nuclear excitation.

Since the electric transition probabilities $B(E2)$ for 2_1^+ states in $^{18,20,22}\text{O}$ isotopes have been measured, we can choose the proton deformation length δ_p so that the experimental transition rate is reproduced by $B_{\text{exp}}(E2 \uparrow) = e^2 |M_p|^2$. As a result, the only free parameter to be determined from the folding model analysis of the (p, p') data is the neutron deformation length δ_n . All the transition matrix elements and other deformation lengths can be directly obtained from δ_p and δ_n using Eqs. (3)-(11). This feature is the main advantage of our folding model approach compared to the standard DWBA or CC analysis using the collective model prescription (2).

We note that the same $^{18,20,22}\text{O}(p, p')$ data have been studied in the folding model using the microscopic nuclear transition densities calculated in the quasiparticle random phase approximation (QRPA) [20]. In these calculations [3, 5, 21], the QRPA proton transition density is scaled to reproduce the experimental $B(E\lambda)$ values, while the strength of the neutron transition density is adjusted to the best DWBA or CC fit to the (p, p') data. The M_n and M_p transition matrix elements given by the ‘scaled’ QRPA transition densities are then compared with the empirical estimates. Since different effective NN interactions were used in the folding calculations of Refs. [3, 5, 21], it is of interest from the reaction theory point of view to probe the microscopic QRPA transition densities in our folding model

analysis using the same effective NN interaction. Therefore, in addition to the BM transition densities (3), we have used in the present work also the QRPA transition densities for 2_1^+ states in Oxygen isotopes given by the continuum QRPA calculation by Khan *et al.* [20] to calculate the inelastic FF. The proton and neutron g.s. densities obtained in the Hartree-Fock-Bogoljubov study [22] were used in the folding model calculation of the proton-nucleus optical potential.

B. Folding model with complex CDM3Y6 interaction

In our version [23] of the folding model, the central nucleon-nucleus potential is evaluated in a Hartree-Fock manner as

$$U = \sum_{j \in A} [\langle ij | v_D | ij \rangle + \langle ij | v_{EX} | ji \rangle], \quad (14)$$

where $v_{D(EX)}$ are the direct and exchange components of the effective NN interaction between the incident nucleon i and nucleon j bound in the target A . The antisymmetrization gives rise to the exchange term in Eq. (14) which makes the nucleon-nucleus potential nonlocal in the coordinate space. To separate the IS and IV contributions, one needs to make explicit the spin- and isospin dependence of the (energy- and density dependent) NN interaction

$$v_{D(EX)}(E, \rho, s) = v_{00}^{D(EX)}(E, \rho, s) + v_{10}^{D(EX)}(E, \rho, s)(\boldsymbol{\sigma}\boldsymbol{\sigma}') \\ + v_{01}^{D(EX)}(E, \rho, s)(\boldsymbol{\tau}\boldsymbol{\tau}') + v_{11}^{D(EX)}(E, \rho, s)(\boldsymbol{\sigma}\boldsymbol{\sigma}')(\boldsymbol{\tau}\boldsymbol{\tau}'), \quad (15)$$

where s is the internucleon distance. The contribution from the spin dependent terms (v_{10} and v_{11}) in Eq. (15) to the central nucleon-nucleus potential (14) is exactly zero for the (spin-saturated) Oxygen targets considered in the present work.

Using a realistic local approximation for the exchange term, the nucleon-nucleus potential (14) can be obtained [23] in terms of the isoscalar (U_{IS}) and isovector (U_{IV}) parts as

$$U(E, \mathbf{R}) = U_{IS}(E, \mathbf{R}) \pm U_{IV}(E, \mathbf{R}), \quad (16)$$

where the $+$ sign pertains to incident neutron and $-$ sign to incident proton. The second term in Eq. (16) is the microscopic expression for the Lane potential in Eq. (1) as well as its prototype in Eq. (2) for the inelastic scattering FF. Each term in Eq. (16) consists of the

corresponding direct and exchange potentials

$$U_{\text{IS}}(E, \mathbf{R}) = \int \{[\rho_n(\mathbf{r}) + \rho_p(\mathbf{r})]v_{00}^{\text{D}}(E, \rho, s) + [\rho_n(\mathbf{R}, \mathbf{r}) + \rho_p(\mathbf{R}, \mathbf{r})]v_{00}^{\text{EX}}(E, \rho, s)j_0(k(E, R)s)\}d^3r, \quad (17)$$

$$U_{\text{IV}}(E, \mathbf{R}) = \int \{[\rho_n(\mathbf{r}) - \rho_p(\mathbf{r})]v_{01}^{\text{D}}(E, \rho, s) + [\rho_n(\mathbf{R}, \mathbf{r}) - \rho_p(\mathbf{R}, \mathbf{r})]v_{01}^{\text{EX}}(E, \rho, s)j_0(k(R)s)\}d^3r, \quad (18)$$

where $\rho(\mathbf{r}, \mathbf{r}')$ is the (one-body) density matrix of the target nucleus, with $\rho(\mathbf{r}) \equiv \rho(\mathbf{r}, \mathbf{r})$. $j_0(x)$ is the zero-order spherical Bessel function and momentum $k(R)$ is determined from

$$k^2(E, R) = \frac{2\mu}{\hbar^2}[E_{\text{c.m.}} - \text{Re } U(R) - V_{\text{C}}(R)]. \quad (19)$$

Here, μ is the nucleon reduced mass, $U(R)$ and $V_{\text{C}}(R)$ are the nuclear and Coulomb parts of the OP, respectively. For a consistent description of the elastic and inelastic nucleon-nucleus scattering, one needs to take into account explicitly the multipole decomposition of the neutron and proton densities that enter the folding calculation (17)-(18). The details of the folding calculation of U_{IS} and U_{IV} are the same as those given in Ref. [23], excepting the use of a realistic local approximation for the *transition* density matrix taken from Ref. [24].

For the effective interaction, we used the density- and isospin dependent CDM3Y6 interaction [14]. While the isoscalar density dependence of the CDM3Y6 interaction has been well tested in the folding model analyses of refractive α -nucleus and nucleus-nucleus scattering (see recent review in Ref. [25]), its *isovector* density dependence was studied only recently in the CC analysis [16, 17] of the charge exchange (p, n) reaction exciting the 0^+ isobaric analog states of targets ranging from ${}^6\text{He}$ to ${}^{208}\text{Pb}$. We recall that the IS density dependence of the CDM3Y6 interaction was introduced [14] as

$$v_{00}^{\text{D(EX)}}(E, \rho, s) = F_{\text{IS}}(E, \rho)v_{00}^{\text{D(EX)}}(s), \quad (20)$$

$$F_{\text{IS}}(E, \rho) = C_0[1 + \alpha_0 \exp(-\beta_0\rho) - \gamma_0\rho], \quad (21)$$

where $v_{00}^{\text{D(EX)}}(s)$ are the direct and exchange components of the isoscalar M3Y-Paris interaction [26]. Parameters of F_{IS} were chosen [14] to reproduce the saturation properties of symmetric nuclear matter in the HF calculation. With a linear energy dependence included into C_0 , the IS interaction (20) reproduces very well the empirical energy dependence of the IS nucleon OP in nuclear matter [27].

For an accurate folding model analysis of the $^{18,20,22}\text{O}(p, p')$ data, it is highly desirable to have a *complex*, density- and isospin dependent NN interaction for the input of the folding calculation (16)-(18). Following Ref. [17], we have constructed in the present work, explicitly for each energy, an imaginary IS density dependence of the same functional form (21) and a complex IV density dependence of the M3Y-Paris interaction

$$v_{01}^{\text{D(EX)}}(E, \rho, s) = F_{\text{IV}}(E, \rho)v_{01}^{\text{D(EX)}}(s), \quad (22)$$

$$F_{\text{IV}}(E, \rho) = C_1[1 + \alpha_1 \exp(-\beta_1 \rho) - \gamma_1 \rho], \quad (23)$$

where the parameters were adjusted to reproduce the JLM density- and isospin dependent nucleon OP [18] in the HF calculation of nuclear matter. All radial shapes of $v_{00(01)}^{\text{D(EX)}}(s)$ were kept unchanged as derived in terms of three Yukawas from the M3Y-Paris interaction [26] (see the explicit expressions for $v_{00(01)}^{\text{D(EX)}}(s)$ in Ref. [15]). The isovector part of the folded proton-nucleus OP has been used in Ref. [17] as the FF for the (p, n) reaction exciting the isobaric analog states, based on the isospin coupling scheme. It turned out [17] that the strength of the real isovector interaction (22) is quite weak to account for the observed (p, n) data and an enhancement of about 20-30% is needed for a good CC description of the (p, n) reaction. Therefore, we have scaled parameter C_1 of the real IV density dependence (23) by a factor of 1.3 before using for the input of the folding calculation (16)-(18). The final parameters of the complex density dependences $F_{\text{IS(IV)}}(E, \rho)$ are presented in Table I. We note that the central proton-nucleus potential (16) is supplemented by the spin-orbital term obtained with the folding method of Ref. [23] and the spin-orbital terms of the CDM3Y6 interaction $v_{LS}^{T=0,1}(\rho, s)$ are assumed to have the same IS and IV density dependences as those used for the central terms. All the optical model (OM) and CC calculations have been performed using the CC code ECIS97 written by Raynal [28].

III. RESULTS AND DISCUSSIONS

A. Transition strength of 2_1^+ state in ^{18}O

For the Oxygen isotopes under study, the 2_1^+ state (at 1.98 MeV) in ^{18}O is the most studied one. The core polarization by the two valence neutrons in the 2_1^+ excitation of ^{18}O was shown to be quite strong, with the M_n/M_p ratio significantly larger than N/Z . The

TABLE I: Parameters of the complex IS and IV density dependence of the CDM3Y6 interaction defined in Eqs. (21) and (23), respectively.

Re $F_{\text{IS}}(E, \rho)$					Im $F_{\text{IS}}(E, \rho)$			
E (MeV)	C_0	α_0	β_0 (fm ³)	γ_0 (fm ³)	C_0	α_0	β_0 (fm ³)	γ_0 (fm ³)
24.5	0.2487	3.8033	1.4099	4.0	0.1504	6.0964	15.503	4.3931
43.0	0.2361	3.8033	1.4099	4.0	0.0869	8.9092	9.9237	4.2128
46.6	0.2336	3.8033	1.4099	4.0	0.1029	6.8937	9.1076	4.2056
Re $F_{\text{IV}}(E, \rho)$					Im $F_{\text{IV}}(E, \rho)$			
E (MeV)	C_1	α_1	β_1 (fm ³)	γ_1 (fm ³)	C_1	α_1	β_1 (fm ³)	γ_1 (fm ³)
24.5	0.2668	6.3227	13.725	-3.8888	0.2010	9.6207	16.053	-4.3670
43.0	0.1490	9.7964	10.743	-4.1147	0.2315	6.2846	13.162	-4.3612
46.6	0.1585	9.3490	11.683	-3.9323	0.2289	6.0590	12.407	-4.4283

neutron transition strength of 2_1^+ state in ^{18}O has been measured in several experiments, like the (direct) inelastic proton and neutron scattering [8, 29, 30] or inelastic pion scattering [31]. The M_n/M_p ratio was often deduced by the (collective model) prescription of Bernstein, Brown and Madsen (BBM) [1] which has been checked against the data collected for a wide range of single-closed shell nuclei. While the BBM analysis of the low-energy proton scattering data seems to favor $M_n/M_p \approx 1.5$ for 2_1^+ state in ^{18}O [2, 4], the inelastic pion scattering data were shown to give a much higher M_n/M_p ratio of 2.3 to 2.4 [31]. The M_n/M_p ratio deduced from the pion scattering data also agrees fairly with that deduced from the measured $B(E2)$ strength of 2_1^+ state in the mirror nucleus ^{18}Ne , using the isospin symmetry [32]. We note that the DWBA analysis of (p, p') and (n, n') scattering data at 24 MeV [8] is of particular interest for our study, as it is the only attempt to determine the IS and IV deformations for 2_1^+ state in ^{18}O prior to our work [12]. By using prescription (2) and assuming δ_0 to be the average of δ values given by the (p, p') and (n, n') data, the authors of Ref. [8] obtained $\delta_0 \approx 1.26 \pm 0.06$ fm and $\delta_1 \approx 3.14 \pm 1.57$ fm which correspond to $M_n/M_p \approx 1.72 \pm 0.70$. The coupled-channel effect at the proton energy of 24 MeV was shown [8] to affect slightly the deduced deformation parameters.


To compare our microscopic folding model analysis of $^{18}\text{O}(p, p')$ data with the collective model results of Ref. [8], we have performed a coupled-channel ($2_1^+ \leftrightarrow 0_{\text{g.s.}}^+ \leftrightarrow 3_1^-$) analysis

of $^{18}\text{O}(p, p')$ data at 24.5 MeV [29] using the (complex) OP and inelastic FF given by the folding calculation (16)-(18) for the lowest 2^+ and 3^- states in ^{18}O . By adjusting M_p to the experimental $B(E2 \uparrow) = 45.1 \pm 2.0 e^2\text{fm}^4$ [33] and $B(E3 \uparrow) = 1120 \pm 11 e^2\text{fm}^6$ [34] for the first 2^+ and 3^- states in ^{18}O , we obtain $\delta_p = 1.04 \pm 0.02$ and 1.45 ± 0.01 fm, respectively, for the corresponding proton transition densities (3). To effectively account for the higher-order dynamic polarization of the OP by the open nonelastic channels, the (complex) strength of the CDM3Y6 interaction is first adjusted to the best CC description of elastic scattering data and then is used without any further renormalization to calculate the inelastic FF. As a result, the only remaining parameter is the neutron deformation length δ_n which is determined from the best CC fit to the inelastic scattering data. The renormalization factors N_R and N_I of the real and imaginary folded OP were first obtained in the OM analysis of the elastic data (see Table II). At 24.5 MeV, the OM fit gives $N_R \approx 0.91$ and $N_I \approx 0.6$. These values have changed slightly to $N_R \approx 0.97$ and $N_I \approx 0.57$ when the two-channel coupling is taken into account. The folded spin-orbital potential needs a renormalization of around 0.5 in both the OM and CC calculations. At higher energy of 43 MeV the best-fit N_R factor becomes close to unity while N_I remains around 0.6. One can see from Fig. 1 that the folded OP gives quite a good description of the measured elastic cross section and analyzing power at 24.5 MeV in both the OM and CC schemes. For a comparison, we have

TABLE II: Renormalization factors N_R and N_I of the real and imaginary folded potentials used in the OM and CC calculations of elastic and inelastic $p+^{18,20,22}\text{O}$ scattering.

OM fit						CC fit		
Target	E (MeV)	N_R	N_I	N_{LS}	σ_R (mb)	N_R	N_I	N_{LS}
^{18}O	24.5	0.91	0.60	0.50	658	0.97	0.57	0.50
^{18}O	43.0	1.00	0.69	0.50	545	1.05	0.64	0.50
^{20}O	43.0	1.08	0.68	0.50	573	1.15	0.60	0.50
^{22}O	46.6	1.00	0.72	0.50	572	1.01	0.70	0.50

also performed the OM calculation using the phenomenological OP (parameterized in terms of Woods-Saxon potentials) taken from an accurate global systematics [35] by Koning and Delaroche (KD). Although KD systematics has been developed for nuclei in the mass range $24 \leq A \leq 209$, our OM analysis shows that it works rather well also for the Oxygen isotopes




Elastic24MeV.eps

FIG. 1: Measured differential cross section and analyzing power of the elastic $p+^{18}\text{O}$ scattering at 24.5 MeV [29] versus the OM results given by the microscopic folded OP and phenomenological OP taken from the global systematics [35] by Koning and Delaroche (KD). The CC results are given by the complex OP and inelastic FF calculated in the folding model.

under study.

The inelastic $p+^{18}\text{O}$ scattering data at 24.5 MeV [29] for 2_1^+ state in ^{18}O are compared with the results of CC calculation in Fig. 2. Like the earlier folding model study [12], we found in the present analysis a significant IV mixing in 2_1^+ excitation which leads to $M_n/M_p \approx 1.55$ (see Table III). This value is about 25% larger than the ratio implied by the isoscalar limit ($M_n/M_p = N/Z = 1.25$). Compared to the elastic channel, the agreement of the CC results with the measured analyzing power of inelastic scattering is rather poor at medium angles, and that could well be due to a simple treatment the inelastic spin-orbital FF adopted in



Inelastic24MeV.eps

FIG. 2: Measured differential cross section and analyzing power of the inelastic $p+^{18}\text{O}$ scattering at 24.5 MeV [29] versus the CC results given by the microscopic folded FF obtained with BM and QRPA transition densities. The collective model result is given by form factor (2) obtained with the phenomenological OP by Koning and Delaroche [35] (see more details in text).

our folding method [23]. However, the inelastic spin-orbital FF does not affect significantly the calculated inelastic 2^+ scattering cross section which is dominated by contribution from the central FF, and the widely accepted procedure is to deduce deformation parameters by matching the calculated inelastic scattering cross section to the data. To stress the reliability of the folding approach, we have done in parallel the same CC calculation but using the collective model form factor (2) determined with the phenomenological OP by Koning and Delaroche [35] and the same IS and IV deformation lengths. As expected, the form factor (2) was found to strongly underestimate the measured 2^+ cross section at large

angles, in about the same way as established earlier in the folding model studies of inelastic heavy-ion scattering [10, 11]. This explains naturally why the IS and IV deformation lengths of 2_1^+ state in ^{18}O deduced by Grabmayr *et al.* [8] in their collective model analysis of the same data ($\delta_0 \approx 1.26$ fm and $\delta_1 \approx 3.14$ fm) are significantly larger than the values deduced from our folding model analysis (see Table III). The numerical uncertainties of δ_p given in



FIG. 3: Elastic and inelastic $p+^{18}\text{O}$ scattering data at 43 MeV [3] in comparison with the OM and CC results. Notations for the OP and inelastic FF are the same as used in Figs. 1 and 2.

Table III are fully determined by those of the measured $B(E2)$ values, while an uncertainty of around 5% was assigned to δ_n which gives a cross-section shift within the experimental errors. The uncertainties of the IS and IV deformation lengths and ratios of transition matrix elements were deduced directly from those found for δ_p and δ_n .

The neutron deformation length found in the CC analysis of the inelastic $p+^{18}\text{O}$ scattering

data at 24.5 MeV has been used to calculate the inelastic $p+^{18}\text{O}$ scattering FF at higher energy of 43 MeV. With only strength of the complex CDM3Y6 interaction slightly adjusted by the CC fit to elastic scattering data, the folding + CC description of the measured (p, p') data at 43 MeV [3] is quite satisfactory (see Fig. 3) without any further adjustment of δ_n for 2_1^+ state in ^{18}O . Given the proton transition strength fixed by the measured $B(E2)$ value, we conclude that the neutron transition matrix element M_n should be such that the ratio $M_n/M_p \approx 1.55$ or equivalently $M_1/M_0 \approx 0.22$. The latter is two times larger than $\varepsilon = 0.11$ and, hence, implies a significant IV mixing in the 2_1^+ excitation. Our present result also agrees closely with that given by the BBM analysis of low-energy proton scattering data ($M_n/M_p \approx 1.5$ for 2_1^+ state in ^{18}O) [2, 4]. The microscopic QRPA transition densities

TABLE III: Deformation lengths and ratios of the transition matrix elements for 2_1^+ states in $^{18,20,22}\text{O}$ deduced from the present folding + CC analysis of inelastic proton scattering [see definitions in Eqs. (3)-(11)].

Nucleus	N/Z	ε	δ_p (fm)	δ_n (fm)	M_n/M_p	δ_0 (fm)	δ_1 (fm)	M_1/M_0
^{18}O	1.25	0.11	1.04 ± 0.02	1.23 ± 0.06	1.55 ± 0.08	1.15 ± 0.04	1.87 ± 0.27	0.22 ± 0.03
^{20}O	1.50	0.20	0.82 ± 0.03	1.95 ± 0.10	3.24 ± 0.20	1.52 ± 0.06	3.75 ± 0.26	0.59 ± 0.05
^{22}O	1.75	0.27	0.70 ± 0.12	0.91 ± 0.05	1.81 ± 0.33	0.85 ± 0.05	1.14 ± 0.16	0.43 ± 0.07

[20] also give a satisfactory description of the inelastic $p+^{18}\text{O}$ scattering data under study (see Figs. 2 and 3). We note that the continuum QRPA calculation of Ref. [20] strongly underestimates the $E2$ strength and gives $B(E2 \uparrow) = 14 e^2\text{fm}^4$ for 2_1^+ state in ^{18}O compared to the experimental value of $45 e^2\text{fm}^4$. On the contrary, the predicted neutron transition strength is much too high ($M_n/M_p \approx 2.88$) compared to that found in the present work and other studies. Such a strong neutron transition strength seems to compensate for the weak proton transition strength predicted by the QRPA, and the inelastic FF folded with the QRPA transition densities gives a reasonable description of the inelastic scattering data. It is interesting that about the same good description of the inelastic scattering data is given by the *renormalized* QRPA densities, with $\rho_2^p(r)$ scaled to reproduce the measured $B(E2)$ value and $\rho_2^n(r)$ scaled to give the same M_n as that obtained above for the BM model (3) of transition densities (see Fig. 2 and lower panel of Fig. 3).

As mentioned above, an alternative method to determine the neutron transition matrix

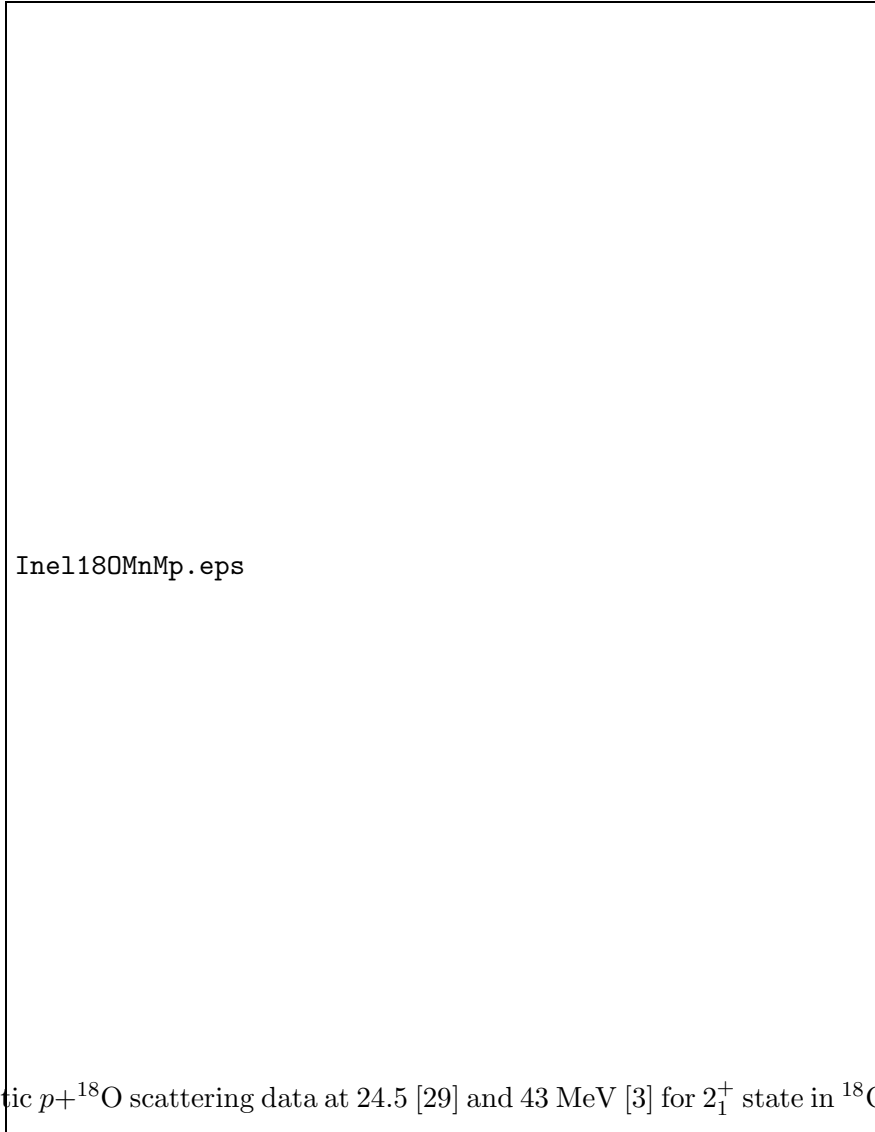


FIG. 4: Inelastic $p+^{18}\text{O}$ scattering data at 24.5 [29] and 43 MeV [3] for 2_1^+ state in ^{18}O in comparison with the CC results. The neutron deformation length δ_n of the transition density (3) was adjusted to give two different ratios $M_n/M_p = 1.55$ and 2.44 .

element M_n has been suggested some 30 years ago by Bernstein *et al.* [32] based on the isospin symmetry. Namely, M_n can be obtained from M_p measured for the same 2^+ excitation in the mirror nucleus with an electromagnetic probe if one assumes the charge independence of the 2^+ excitation in members of a T -isospin multiplet. In particular, one has for the isobars with opposite signs of the isospin projection T_z

$$M_p(-T_z) = M_n(T_z). \quad (24)$$

Using the electric transition rates $B(E2)$ for ^{18}O and ^{18}Ne taken from the latest compilation of the experimental data [33], we easily deduce the ratio of transition matrix elements

$M_n/M_p \approx 2.44 \pm 0.18$ for 2_1^+ states in ^{18}O using Eq. (24). This value is significantly larger than that obtained in the present folding + CC analysis and collective model analyses reported in Refs. [2, 4, 8]. To illustrate such a difference in terms of the (p, p') cross section, we have done the same folding + CC calculation but using the *enhanced* neutron transition density (3) which gives $M_n/M_p \approx 2.44$. Then, the calculated inelastic cross sections strongly overestimate the measured (p, p') data at both energies under study (see Fig. 4). Assuming the realistic value $M_n/M_p \approx 1.55$, we might interpret the difference shown in Fig. 4 as an indication to the isospin impurity in the 2_1^+ excitations of the $A = 18$, $T = 1$ isobaric multiplet. It is complementary to note that a similar isospin-impurity effect has been found by Khan *et al.* [36] for the 2_1^+ excitations of the $A = 30$, $T = 1$ isobaric multiplet. Nevertheless, if one takes into account the data of inelastic π^+ and π^- scattering from ^{18}O [31] which give $M_n/M_p \approx 2.3 - 2.4$ in a distorted-wave impulse approximation analysis using different types of the transition density for 2_1^+ state, then the measured $B(E2)$ value of 2_1^+ state in the mirror ^{18}Ne nucleus seems to support a good isospin symmetry in this case. Given the accurately measured electric transition rates $B(E2)$ of 2_1^+ states in ^{18}O and ^{18}Ne , a future (high-precision) experiment to re-determine the neutron transition strengths of 2_1^+ states in these two mirror nuclei should provide vital data for the determination of the isospin impurity using relation (24).

B. Transition strength of 2_1^+ state in ^{20}O

In difference from the stable ^{18}O target, inelastic proton scattering to 2_1^+ state in the *unstable* ^{20}O isotope has been measured only recently, in the inverse kinematics, at 30 MeV [2] and 43 MeV [3]. Using the measured transition rate $B(E2 \uparrow) \approx 28.1 \pm 2.0 e^2\text{fm}^4$ [33] for 2_1^+ state in ^{20}O , we have deduced the proton deformation length $\delta_p \approx 0.82 \pm 0.03$ fm for the proton transition density (3). The proton deformation length of 3_1^- state in ^{20}O was taken from the empirical estimate of Ref. [12], and the neutron deformation length was then adjusted to the best CC fit to the inelastic $^{18}\text{O}(p, p')$ data for 3_1^- excitation [3]. Similar to our earlier folding + DWBA analysis [12] of these data, the best-fit M_n/M_p ratio for the 3_1^- excitation turned out to be quite close to $N/Z = 1.5$ which indicates a dominant IS character of this state. The isospin character of 2_1^+ state is very much different from that found for 3_1^- state. Using the deformation parameters extracted from the CC analysis of the 30 MeV

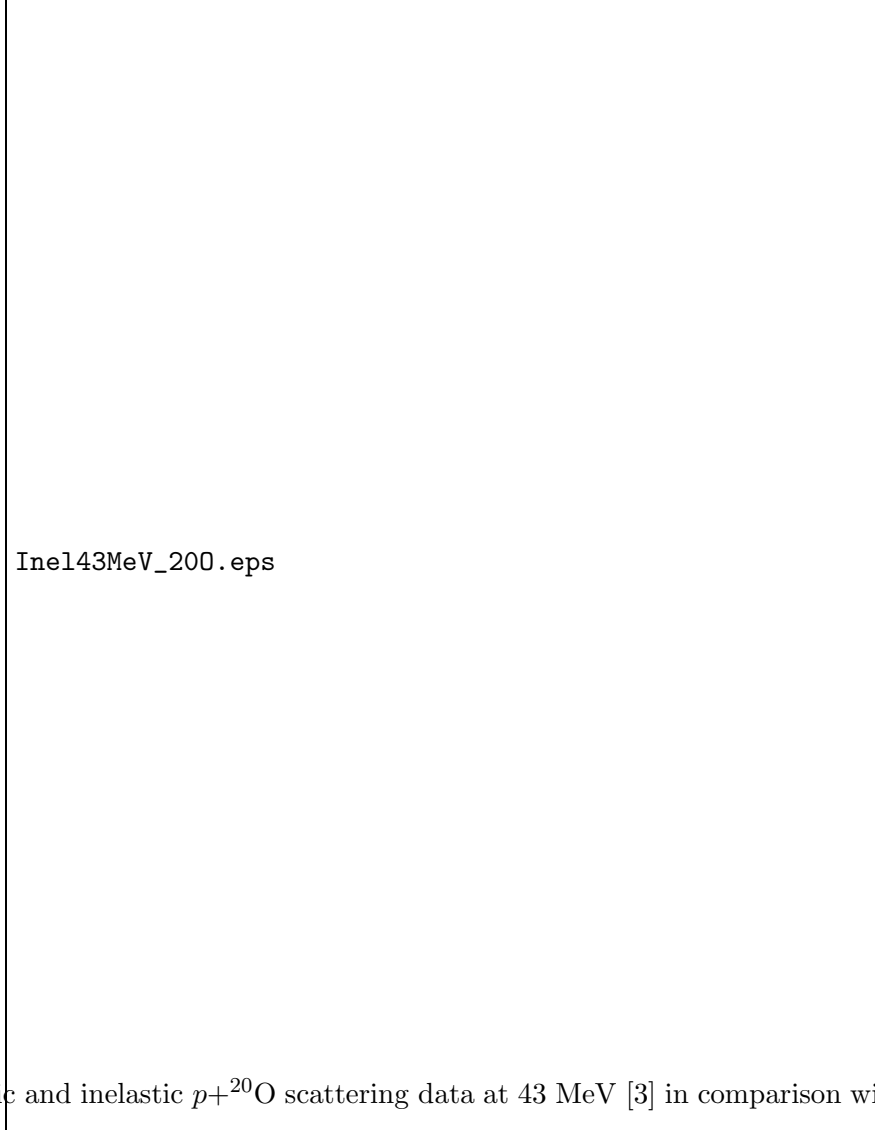


FIG. 5: Elastic and inelastic $p+^{20}\text{O}$ scattering data at 43 MeV [3] in comparison with the OM and CC results. Notations for the OP and inelastic FF are the same as used in Figs. 1 and 2.

data with the collective model FF, the ratio of neutron/proton transition matrix elements $M_n/M_p \approx 2.9 \pm 0.4$ has been deduced by Jewell *et al.* [2] for 2_1^+ state in ^{20}O . The JLM folding model analysis of 43 MeV data by Khan *et al.* [3] using the QRPA transition densities has found a stronger IV mixing in this state, with $M_n/M_p \approx 3.25 \pm 0.80$. Our earlier folding model analysis [12], using the compact method (3)-(11) and original CDM3Y6 interaction with the IV density dependence assumed to be the same as the IS one, has given a larger ratio of $M_n/M_p \simeq 4.2$ for 2_1^+ states in ^{20}O . In the present work we concentrate on the 43 MeV data which contain more data points and cover a wider angular range. The results of our folding + CC analysis are compared with the elastic and inelastic $p+^{20}\text{O}$ scattering data at 43 MeV in Fig. 5. With δ_p fixed above by the measured $B(E2)$ value, the best-fit

neutron deformation length is $\delta_n \approx 1.95$ fm which results on the ratios $M_n/M_p \approx 3.24$ and $M_1/M_0 \approx 0.59$. These values are well exceeding the IS limit of $M_n/M_p \approx N/Z = 1.5$ and $M_1/M_0 \approx \varepsilon = 0.2$. The deduced IV deformation length (see Table III) is about 2.5 times the IS deformation length and confirms, therefore, a strong core polarization by the valence neutrons in 2_1^+ excitation of the *open-shell* ^{20}O nucleus. In difference from the inelastic $p+^{18}\text{O}$ scattering data at 24.5 MeV shown in Fig. 2, the 43 MeV data for $^{18,20}\text{O}$ ‘targets’ (measured at angles $\Theta_{\text{c.m.}} < 50^\circ$ only) are reasonably reproduced by both the folded and collective model form factors based on the same δ_0 and δ_1 . A substantial difference between the CC results given by these two choices of inelastic FF was found at larger scattering angles ($50^\circ < \Theta_{\text{c.m.}} < 180^\circ$) where no data point was taken. In this sense, a future experiment aiming to measure (p, p') cross section over a wider angular range could provide a better test ground for the inelastic FF and neutron transition strength.

The continuum QRPA description of 2_1^+ state in ^{20}O is better than that for ^{18}O , with the predicted $B(E2 \uparrow) \approx 22 e^2\text{fm}^4$ (compared to the adopted experimental value of $28 e^2\text{fm}^4$) and $M_n/M_p \approx 3.36$ [20]. A good CC description of the (p, p') cross section was obtained after a slight renormalization of the QRPA transition densities to reproduce the experimental $B(E2)$ value and best-fit M_n/M_p ratio (see Fig. 5). We stress that the use of a more realistic version of the (complex) density- and isospin dependent CDM3Y6 interaction in the present work has pinned down the best-fit ratio of transition matrix elements for 2_1^+ state in ^{20}O to $M_n/M_p \approx 3.24$ which is very close to that deduced from the JLM folding model analysis [3] of the same data. Together with the results of the BBM analysis reported in Refs. [2, 4], our results confirm again a strong IV mixing in 2_1^+ excitation of ^{20}O .

Like the ^{18}O case, there is an alternative method to determine the M_n/M_p ratio from the electric $B(E2)$ transition rates measured for 2_1^+ states in ^{20}O and its mirror partner ^{20}Mg , using Eq. (24) given by the isospin symmetry. Towards this goal, a measurement of the Coulomb excitation of the unstable ^{20}Mg nucleus has been performed by RIKEN group [6] using a radioactive ^{20}Mg beam incident on the lead target. The extracted transition rate $B(E2 \uparrow) \approx 177 \pm 32 e^2\text{fm}^4$ for 2_1^+ state in ^{20}Mg seems to agree well with the prediction of realistic cluster model for this nucleus. Assuming the proton transition matrix element M_p for 2_1^+ state in ^{20}Mg equal the neutron transition matrix element M_n for 2_1^+ state in ^{20}O , one obtains easily $M_n/M_p \approx 2.51 \pm 0.25$ for the latter. This value is about 30% smaller than the best-fit M_n/M_p ratio obtained in Ref. [3] and present work. Given an accurate

treatment of the folding model ingredients and similar effect discussed above for 2_1^+ state in ^{18}O , such a difference in M_n/M_p ratios deduced by the two methods might well indicate the isospin impurity in the 2_1^+ excitation of the $A = 20$, $T = 2$ isobaric multiplet. To



Inel200MnMp.eps

FIG. 6: Inelastic $p+^{20}\text{O}$ scattering data at 43 MeV [3] for 2_1^+ state in ^{20}O in comparison with the CC results. The neutron deformation length δ_n of the transition density (3) was adjusted to give two different ratios $M_n/M_p = 2.51$ and 3.24 .

illustrate this effect in the calculated inelastic cross sections, we have plotted in Fig. 6 the CC result obtained with two choices of the neutron transition density (3) which were scaled to give $M_n/M_p \approx 2.51$ and 3.24 . One can see that the CC results associated with $M_n/M_p \approx 2.51$ substantially underestimate the measured (p, p') data. In terms of the total (p, p') cross section, the difference caused by the ‘isospin impurity’ shown in Fig. 6 is around 40%. This difference reduces to around 30% when one adopts the upper limit of the measured transition rate, $B(E2 \uparrow) \approx 210 e^2\text{fm}^4$, for 2_1^+ state in ^{20}Mg [6]. We must note, however, that the last 2 data points in Fig. 6 seem to agree better with the CC results associated with $M_n/M_p \approx 2.51$. In the same logic as discussed above for ^{18}O and ^{18}Ne , a future *inverse-kinematics* measurement of $^{20}\text{O}(p, p')$ and $^{20}\text{Mg}(p, p')$ reactions to determine neutron transition strength of 2_1^+ states in these two mirror *unstable* nuclei could provide

important data for the check of isospin purity in the 2_1^+ excitation of the $A = 20$, $T = 2$ isobars using relation (24).

C. Transition strength of 2_1^+ state in ^{22}O

If we consider ^{20}O as consisting of the ^{16}O core and four valence neutrons, then the large IV deformation length δ_1 extracted above for 2_1^+ state in ^{20}O indicates a strong core polarization by the valence neutrons in the 2_1^+ excitation. In such a ‘core + valence neutrons’ picture, it is natural to expect that 2_1^+ state in ^{22}O should be more collective and have a larger IV deformation length due to the contribution of two more valence neutrons. However, the inelastic $^{22}\text{O}(p, p')$ scattering data at 46.6 MeV measured recently at GANIL [5] show clearly the opposite effect, with the inelastic cross section about 3 to 4 times smaller than $^{22}\text{O}(p, p')$ cross section measured at 43 MeV [3] for 2_1^+ state in ^{20}O . The folding + DWBA analysis [5] of these data using the method (3)-(11) and original CDM3Y6 interaction (with the IV density dependence assumed to be the same as the IS one) has pointed to a much weaker neutron transition strength of 2_1^+ in ^{22}O . Given a significantly higher excitation energy of this state (1.5 MeV higher than that of 2_1^+ state in ^{20}O), the $^{22}\text{O}(p, p')$ data at 46.6 MeV were considered [5] as an important evidence for the neutron shell closure occurring at $N = 14$ or 16. Given the measured transition rate $B(E2 \uparrow) \approx 21 \pm 8 e^2\text{fm}^4$ [33] for 2_1^+ state in ^{22}O , we have obtained the proton deformation length $\delta_p \approx 0.70 \pm 0.12$ fm for the proton transition density (3). Like in cases of $^{18,20}\text{O}$, the neutron deformation length for 2_1^+ state in ^{20}O was adjusted to the best description of the 46.6 MeV data by the folding + CC analysis. Since there are no data measured for (p, p') scattering at 46.6 MeV to 3_1^- state in ^{22}O , we have considered in our CC scheme only the coupling between the elastic and 2^+ inelastic scattering channels ($0_{\text{g.s.}}^+ \leftrightarrow 2_1^+$). The folding + CC results are compared with the elastic and inelastic $p+^{22}\text{O}$ scattering data in Fig. 7. With δ_p fixed by the measured $B(E2)$ value, the best-fit neutron deformation length was found $\delta_n \approx 0.9$ fm which lead to the ratios $M_n/M_p \approx 1.81$ and $M_1/M_0 \approx 0.43$. These values are rather close to those implied by the IS limit of $M_n/M_p \approx N/Z = 1.75$ and $M_1/M_0 \approx \varepsilon = 0.27$. The deduced IV deformation length δ_1 is around 30% larger than the IS deformation length δ_0 (see Table III) and this is much smaller than the difference between δ_1 and δ_0 found above for 2_1^+ state in ^{20}O . Thus, our results show a much weaker polarization effect by the valence neutrons in

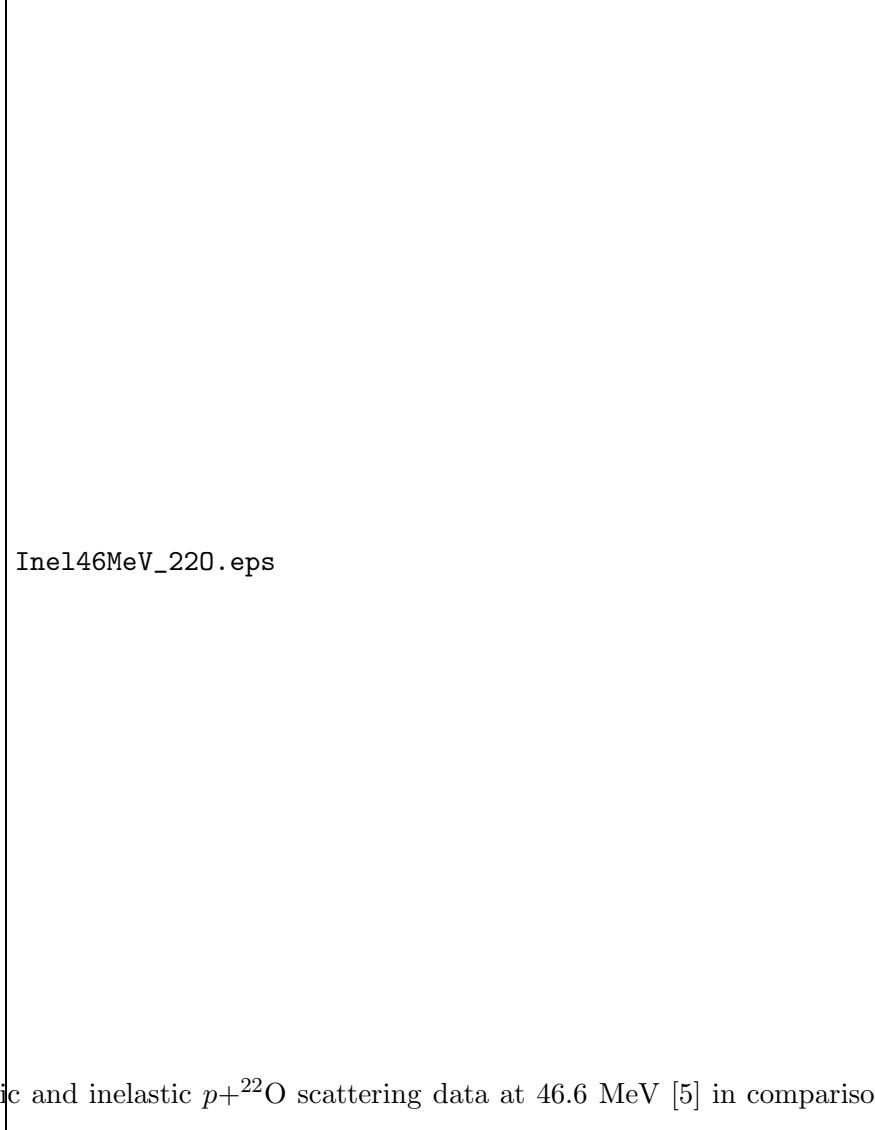


FIG. 7: Elastic and inelastic $p+^{22}\text{O}$ scattering data at 46.6 MeV [5] in comparison with the OM and CC results. Notations for the OP and inelastic FF are the same as used in Figs. 1 and 2.

the 2_1^+ excitation of ^{22}O nucleus. This subtle effect could not be accurately described by the continuum QRPA. While the QRPA calculation gives $B(E2 \uparrow) \approx 22 e^2\text{fm}^4$ (in a perfect agreement with the measured value [33]), the predicted $M_n/M_p \approx 3.53$ [20] is nearly two times the empirical data. That is the reason why the CC results given by the original QRPA transition densities for 2_1^+ state in ^{22}O strongly overestimate the data as shown in Fig. 7. Like the ^{20}O case, the inelastic $p+^{22}\text{O}$ data are reasonably reproduced by both the folded and collective model FF based on the same deformation IS and IV lengths. A significant difference given by the two choices of inelastic FF can be seen at larger scattering angles where no data point was measured.

Given a smaller IV deformation resulted from a weaker core polarization by the valence




FIG. 8: Inelastic $p+^{20,22}\text{O}$ scattering data versus the CC results given by inelastic folded FF with the isospin dependence of the CDM3Y6 interaction included (IS+IV) or neglected (IS only).

neutrons in 2_1^+ excitation of ^{22}O compared to the ^{20}O case, it is quite illustrative to show the explicit IV contribution in the calculated inelastic cross section. We have plotted in Fig. 8 the calculated inelastic $p+^{20,22}\text{O}$ cross sections given by inelastic folded FF with the contribution from the isovector part (18) included or neglected. One can see that the IV contribution is very strong and amounts up to 40% of the total inelastic cross section in the ^{20}O case, and it becomes weaker (around 22%) in the ^{22}O case. As can be seen from Eq. (18), the IV part of the folded FF is entirely determined by the difference between the neutron and proton transition densities and its strength is, therefore, directly proportional to the contribution by the valence neutrons. Consequently, it is vital to treat the IV dependence of the (effective) NN interaction properly in a folding model analysis of proton scattering on a neutron-rich

target before the neutron transition strength can be accurately deduced. Although one could still obtain a good description of the (p, p') data with the IS form factor only by scaling up the strength of transition densities, like in the folding model analysis [21] of these same data using the same continuum QRPA transition densities and *isospin independent* DDM3Y interaction, it is uncertain to compare the best-fit M_n/M_p ratios obtained in such an analysis with those deduced by our consistent folding method. Finally, it is interesting to note that the contribution by the IV form factor to the (p, p') cross section for 2_1^+ excitation of ^{20}O is very close to the cross section shift presumably caused the ‘isospin impurity’ in the 2_1^+ excitation of the $A = 20$, $T = 2$ isobars (compare Fig. 6 and upper panel of Fig. 8).

With a direct connection between the IV deformation and dynamic contribution by the valence neutrons to the nuclear excitation, it is natural to link the IV deformation with possible changes of the neutron shell structure. The best-fit IS and IV deformation lengths of 2_1^+ states in Oxygen isotopes and those derived from the results of continuum QRPA calculation [20], using Eqs. (9) and (10), are plotted versus the neutron number N in Fig. 9. For the double-closed shell ^{16}O nucleus, we have adopted the IS limit with $\delta_0 = \delta_1 = 1.038 \pm 0.048$ fm as deduced from the measured $B(E2)$ value and used in a recent folding model study of inelastic $^{16}\text{O}+^{16}\text{O}$ scattering [37]. An enhanced IV deformation (with $\delta_1 > \delta_0$) resulted from the core polarization by the valence neutrons can be seen for the open-shell $^{18,20}\text{O}$ nuclei, with maximum of δ_1 observed for 2_1^+ state in ^{20}O or at $N = 12$. Such a maximum of the IV deformation also corresponds to the largest M_n/M_p ratio found for 2_1^+ state in ^{20}O . With N approaching 14, the extracted δ_1 value is drastically reduced and becomes rather close to δ_0 which indicates a much weaker IV mixing in 2_1^+ excitation of ^{22}O . A similar trend has also been predicted by the continuum QRPA calculation [20], although the predicted difference between δ_1 and δ_0 still remains significant at $N = 14$. This difference was predicted to be substantially smaller at $N = 16$ (see open squares and circles in Fig. 9), and it is natural to suggest from the N -dependence shown in Fig. 9 that δ_1 is reaching its second minimum at $N = 16$. Based on a similar N dependence obtained for the IV deformation lengths of 2_1^+ states in Sulfur isotopes [13] where a clear minimum of δ_1 was found at the neutron magic number $N = 20$, the deduced N dependence of δ_1 for 2_1^+ states in Oxygen isotopes seems to suggest that the neutron shell closure occurs again at $N = 16$ in Oxygen isotopes. Such a shell closure scenario is well illustrated by the N dependence of the excitation energies of 2_1^+ states in Oxygen isotopes (upper panel of Fig. 9). One



Ex_Delta01.eps

FIG. 9: Observed excitation energies (upper panel), the isoscalar (δ_0) and isovector (δ_1) deformation lengths (lower panel) of 2_1^+ states in Oxygen isotopes deduced from the folding model analyses of this work and Ref. [37] (for double-closed shell ^{16}O) and from the continuum QRPA results [20].

can see that the energy of 2_1^+ state goes through its minimum at $N = 12$, where the core polarizing contribution by the valence neutrons is strongest. As N moves to $N = 16$ this contribution becomes much weaker and the excitation energy of 2_1^+ state becomes larger because of the *enhanced* energy gap between the $1s$ and $0d$ neutron subshells. Although the excitation energy of 2_1^+ state in ^{24}O was predicted by different structure calculations [20, 38] to be around 4 MeV, the experimental observation has been quite difficult due to the weak excitation of this state. In particular, no (p, p') data could be measured so far for 2_1^+ state in ^{24}O . An important evidence has been found recently in the experiment on neutron decay of unstable Oxygen isotopes by Frank *et al.* [39], where 2_1^+ state of ^{24}O was identified as a very

weak resonance at the excitation energy of about 4.8 MeV which undergoes direct neutron decay to the ground state of ^{23}O . Assuming the weak $E2$ transition strength predicted by the continuum QRPA [20] for 2_1^+ state in ^{24}O , our folding model approach predicts that the (p, p') cross section for this state is at least factor of 2 smaller than that measured for 2_1^+ state in ^{22}O [5]. The (unbound) excited $5/2^+$ state of ^{23}O has also been observed in the same neutron decay measurement [39] at an excitation energy of around 2.8 MeV which fits well into the gap of about 4 MeV between the $1s_{1/2}$ and $0d_{3/2}$ subshells predicted, e.g., by the Hartree-Fock-Bogoljubov calculation [38]. Based on this discussion as well as the systematics on the β -decay Q values and single neutron separation energies made by Kanungo *et al.* [40] for a wide range of neutron rich even-even isotopes, we can draw a definitive conclusion on the neutron shell closure at $N = 16$ in unstable Oxygen isotopes. To this end, more experiments for ^{24}O , especially, the (p, p') measurement in the inverse kinematics would be of further interest.

IV. SUMMARY

A coupled channel analysis of the $^{18,20,22}\text{O}(p, p')$ scattering data has been performed, using the OP and inelastic FF calculated microscopically in a compact folding model approach, to extract the neutron transition matrix elements M_n as well as the isoscalar (δ_0) and isovector (δ_1) deformation lengths of 2_1^+ states in the Oxygen isotopes, with the proton transition matrix elements M_p fixed by the measured electric transition rates $B(E2)$.

The newly determined ratios M_n/M_p for 2_1^+ states in $^{18,20}\text{O}$ have been compared to those deduced from the isospin symmetry, using the experimental $B(E2)$ transition rates of 2_1^+ states in the proton rich ^{18}Ne and ^{20}Mg isotopes. Given the experimental $B(E2)$ values available for 2_1^+ states in these four nuclei, a future high-precision (p, p') measurement to accurately determine the neutron transition strengths of 2_1^+ states in the mirror pairs $^{18}\text{O}, ^{18}\text{Ne}$ and $^{20}\text{O}, ^{20}\text{Mg}$ (in the inverse kinematics), should provide vital information on the isospin impurity in the 2_1^+ excitation of $A = 18, T = 1$ and $A = 20, T = 2$ isobaric multiplets, respectively.

The enhancement of the IV deformation has been confirmed again for the open-shell $^{18,20}\text{O}$ nuclei which show a strong core polarization by the valence neutrons. Along the isotope chain, the behavior of the dynamic IV deformation of 2_1^+ state is closely correlated

with the evolution of the valence neutron shell, and δ_1 has been found to reach its maximum at $N = 12$ which corresponds to the largest M_n/M_p ratio found for 2_1^+ state in ^{20}O . A fast decrease of the IV deformation towards $N = 16$ should be connected with the neutron shell closure occurring at this new magic number of neutrons.

Acknowledgement

The authors thank Elias Khan for helpful communications on the $^{18,20,22}\text{O}(p, p')$ data and QRPA results for the nuclear transition densities. N.D.C. is grateful to H.S. Than for his assistance in the numerical calculation. The research was supported, in part, by Natural Science Council of Vietnam and Vietnam Atomic Energy Commission (VAEC).

-
- [1] A.M. Bernstein, V.R. Brown, and V.A. Madsen, *Comments Nucl. Part. Phys.*, **11**, 203 (1983).
 - [2] J.K. Jewell, L.A. Riley, P.D. Cottle, K.W. Kemper, T. Glasmacher, R.W. Ibbotson, H. Scheit, M. Chromik, Y. Blumenfeld, S.E. Hirzebruch, F. Maréchal, and T. Suomijärvi, *Phys. Lett. B* **454**, 181 (1999).
 - [3] E. Khan, Y. Blumenfeld, N.V. Giai, T. Suomijärvi, N. Alamanos, F. Auger, G. Colò, N. Francaria, A. Gillibert, T. Glasmacher, M. Godwin, K.W. Kemper, V. Lapoux, I. Lhenry, F. Maréchal, D.J. Morrissey, A. Musumarra, N.A. Orr, S. Ottini-Hustache, P. Piattelli, E.C. Pollacco, P. Roussel-Chomaz, J.C. Roynette, D. Santonocito, J.E. Sauvestre, J.A. Scarpaci, and C. Volpe, *Phys. Lett. B* **490**, 45 (2000).
 - [4] P.D. Cottle, *Nucl. Phys.* **A682**, 124c (2001).
 - [5] E. Becheva, Y. Blumenfeld, E. Khan, D. Beaumel, J.M. Daugas, F. Delaunay, Ch-E. Demonchy, A. Drouart, M. Fallot, A. Gillibert, L. Giot, M. Grasso, N. Keeley, K.W. Kemper, D.T. Khoa, V. Lapoux, V. Lima, A. Musumarra, L. Nalpas, E.C. Pollacco, O. Roig, P. Roussel-Chomaz, J.E. Sauvestre, J.A. Scarpaci, F. Skaza, and H.S. Than, *Phys. Rev. Lett.* **96**, 012501 (2006).
 - [6] N. Iwasa, T. Motobayashi, S. Bishop, Z. Elekes, J. Gibelin, M. Hosoi, K. Ieki, K. Ishikawa, H. Iwasaki, S. Kawai, S. Kubono, K. Kurita, M. Kurokawa, N. Matsui, T. Minemura, H. Morikawa, T. Nakamura, M. Niikura, M. Notani, S. Ota, A. Saito, H. Sakurai, S. Shimoura,

- K. Sugawara, T. Sugimoto, H. Suzuki, T. Suzuki, I. Tanihata, E. Takeshita, T. Teranishi, Y. Togano, K. Yamada, K. Yamaguchi, and Y. Yanagisawa, *Phys. Rev. C* **78**, 024306 (2008).
- [7] A.M. Lane, *Phys. Rev. Lett.* **8**, 171 (1962).
- [8] P. Grabmayr, J. Rapaport, and R.W. Finlay, *Nucl. Phys.* **A350**, 167 (1980).
- [9] R.W. Finlay, J. Rapaport, V.R. Brown, V.A. Madsen, and J.R. Comfort, *Phys. Lett.* **84B**, 169 (1979).
- [10] J.R. Beene, D.J. Horen, and G.R. Satchler, *Phys. Lett. B* **344**, 67 (1995); *Nucl. Phys.* **A596**, 137 (1996).
- [11] D.T. Khoa and G.R. Satchler, *Nucl. Phys.* **A668**, 3 (2000).
- [12] D.T. Khoa, *Phys. Rev. C* **68**, 011601(R) (2003).
- [13] D.T. Khoa, *Eur. Phys. J. Special Topics* **150**, 31 (2007).
- [14] D.T. Khoa, G.R. Satchler, and W. von Oertzen, *Phys. Rev. C* **56**, 954 (1997).
- [15] D.T. Khoa, W. von Oertzen, and A. A. Ogloblin, *Nucl. Phys.* **A602**, 98 (1996).
- [16] D.T. Khoa and H.S. Than, *Phys. Rev. C* **71**, 044601 (2005).
- [17] D.T. Khoa, H.S. Than, and D.C. Cuong, *Phys. Rev. C* **76**, 014603 (2007).
- [18] J.P. Jeukenne, A. Lejeune, and C. Mahaux, *Phys. Rev. C* **16**, 80 (1977).
- [19] A. Bohr and B.R. Mottelson, *Nuclear Structure* (Benjamin, New York, 1975), Vol.2.
- [20] E. Khan, N. Sandulescu, M. Grasso, and N.V. Giai, *Phys. Rev. C* **66**, 024309 (2002).
- [21] D. Gupta, E. Khan, and Y. Blumenfeld, *Nucl. Phys.* **A773**, 230 (2006).
- [22] M. Grasso, N. Sandulescu, N.V. Giai, and R.J. Liotta, *Phys. Rev. C* **64**, 064321 (2001).
- [23] D.T. Khoa, E. Khan, G. Colò, and N.V. Giai, *Nucl. Phys.* **A706**, 61 (2002).
- [24] W.G. Love, *Nucl. Phys.* **A312**, 160 (1978).
- [25] D.T. Khoa, W. von Oertzen, H.G. Bohlen, and S. Ohkubo, *J. Phys. G* **34**, R111 (2007).
- [26] N. Anantaraman, H. Toki, and G.F. Bertsch, *Nucl. Phys.* **A398**, 269 (1983).
- [27] D.T. Khoa and W. von Oertzen, *Phys. Lett. B* **304**, 8 (1993); D.T. Khoa and W. von Oertzen, *Phys. Lett. B* **342**, 6 (1995).
- [28] J. Raynal, *Computing as a Language of Physics* (IAEA, Vienna, 1972) p.75; J. Raynal, coupled-channel code ECIS97 (unpublished).
- [29] J.L. Escudie, R. Lombard, M. Pignanelli, F. Resmini, and A. Tarrats, *Phys. Rev. C* **10**, 1645 (1974).
- [30] J. Kelly, W. Bertozzi, T.N. Buti, J.M. Finn, F.W. Hersman, M.V. Hynes, C. Hyde-Wright,

- B.E. Norum, A.D. Bacher, G.T. Emery, C.C. Foster, W.P. Jones, D.W. Miller, B.L. Berman, J.A. Carr, and F. Petrovich, *Phys. Lett.* **169B**, 157 (1986).
- [31] S.J. Seestrom-Morris, D. Dehnhard, M.A. Franey, D.B. Holtkamp, C.L. Blilie, C.L. Morris, J.D. Zumbro, and H.T. Fortune, *Phys. Rev. C* **37**, 2057 (1988).
- [32] A.M. Bernstein, V.R. Brown, and V.A. Madsen, *Phys. Rev. Lett.* **42**, 425 (1979).
- [33] S. Raman, C. W. Nestor, Jr., and P. Tikkanen, *At. Data and Nucl. Data Tables* **78**, 1 (2001).
- [34] R.H. Spear, *At. Data and Nucl. Data Tables* **42**, 55 (1989).
- [35] A.J. Koning and J.P. Delaroche, *Nucl. Phys.* **A713**, 231 (2003).
- [36] E. Khan, V. Lapoux, N. Alamanos, and Y. Blumenfeld, *Phys. Rev. C* **69**, 031303(R) (2004).
- [37] D.T. Khoa, H.G. Bohlen, W. von Oertzen, G. Bartnitzky, A. Blazevic, F. Nuoffer, B. Gebauer, W. Mittig, and P. Roussel-Chomaz, *Nucl. Phys.* **A759**, 3 (2005).
- [38] A. Obertelli, S. Peru, J.-P. Delaroche, A. Gillibert, M. Girod, and H. Goutte, *Phys. Rev. C* **71**, 024304 (2005).
- [39] N. Frank, T. Baumann, D. Bazin, B.A. Brown, J. Brown, P.A. DeYoung, J.E. Finck, A. Gade, J. Hinnefeld, R. Howes, J.L. Lecouey, B. Luther, W.A. Peters, H. Scheit, A. Schiller, M. Thoennessen, and J. Tostevin, *Nucl. Phys.* **A813**, 199 (2008).
- [40] R. Kanungo, I. Tanihata, and A. Ozawa, *Phys. Lett. B* **528**, 58 (2002).

